Deeper insights into the density functional theory of structural, optical, and photoelectrical properties using 5-[(4-oxo-4H-chromen-3-yl) methylidene]-4-oxo (thioxo)-6-thioxo-2-sulfido-1, 3, 2-diazaphosphinanes

Shimaa Abdel Halim[1] · Hesham Hamad[2] · Tarik E. Ali[1,3]

Abstract

The structure–activity relationship studied by DFT calculations and contacted with practical antimicrobial results for compounds **1–4** is discussed in detail. In light of this compounds **1–4** have been studied by using DFT/B3LYB/6-311++G (d,p) at the level of theory, the geometrical parameters, bond lengths and bond angles have been discussed. The results of quantum mechanical calculations showed that the presence of phosphorus and sulfur atoms changed the planarity of the parent compound **1** by the range from -11 to 125°. The electronic parameter and dipole moment of these compounds in the ground state theoretically is analyzed by computing HOMO and LUMO pictures. Using frontier molecular orbital analysis, various spectroscopic and quantum chemical parameters are evaluated. Besides, absorption energies, oscillator strength, and electronic transitions of 1,3,2-diazaphosphinines **1–4** molecules have been derived at TD-DFT/CAM-B3LYP/6-311++G (d,p) computations utilizing, then the CAM-B3LYP method is "the Coulomb-attenuating method bases" set studied the electronic absorption spectra theoretically in the gas phase (TD-DFT) with the polarized split-valence 6-311++G (d, p) basis sets, in addition, the corrected linear response polarizable continuum model and measured experimentally in methanol and cyclohexane indicate a good agreement with the observed spectra (practically) in UV–Vis spectra. The molecular electrostatic potential surfaces plots have been computed to understand reactivity points.

Keywords 1,2,3-diazaphosphinanes · DFT/TD-DFT · NLO/NBO analysis · Optoelectronic application

✉ Shimaa Abdel Halim
shimaabdelhalim@edu.asu.edu.eg

✉ Hesham Hamad
heshamaterials@hotmail.com

1 Department of Chemistry, Faculty of Education, Ain Shams University, Roxy, Cairo 11711, Egypt

2 Fabrication Technology Research Department, Advanced Technology and New Materials Research Institute (ATNMRI), City of Scientific Research and Technological Applications (SRTA-City), P.O. Box 21934, New Borg El-Arab City, Alexandria, Egypt

3 Department of Chemistry, Faculty of Science, King Khalid University, Abha, Saudi Arabia

1 Introduction

Organic molecule compounds' optoelectronic properties, which mostly depend on excitons generation, are increasingly generating more interest due to low cost and simple fabrication procedures, a variety of application areas, and large-scale production (El-Remaily et al. 2023). In addition, some of these organic molecules have different biological activities. 1, 3, 2-Diazaphosphinines are an important class of organophosphorus family in recent years due to their biological properties (Hassanin et al. 2018). They are considered antiproliferative (Long et al. 2008), enzyme inhibitory (Wang et al. 2012), antibiotic (Dake et al. 2011), analgesic (Abdou et al. 2012), and as promising anticancer therapeutic drugs (Akbas et al. 2013). On the other hand, chromone compounds are well-known natural and synthetic products that showed significant biological activities including antiallergic (Nohara et al. 1985), antiangiogenic (Lee et al. 2005), antirheumatic (Ukawa, et al. 1985), antitumor (Huang et al. 2009), neuroprotective (Larget et al. 2000), HIV-inhibitory (Ungwitayatorn et al. 2004), antimicrobial (Göker et al. 2005), antioxidant (Pietta et al. 2000), and anti-inflammatory (Mazzei et al. 1999). Appropriately, it seems, by all accounts, to be exceedingly appealing to study the previously synthesized 1,2,3-diazaphosphinines bearing a chromone ring **1–4** of biological intrigue from a computational investigation point of view (Ali and Hassan 2018). It has been uncovered those compounds containing 1,3,2-diazaphosphinines structures display noteworthy biological properties, which have attracted many researchers' attention in chemical biology and medicinal chemistry.

Density functional theory based computational study play a vital role in identifying the new drug candidates. There is no reported systematic study on the UV–Vis spectra of 1,2,3-diazaphosphinanes bearing a chromone ring. Thus, the present work attempts to provide a comprehensive study of experimental UV–Vis spectra for these compounds using Time-Dependent Density Functional Theory (TD-DFT) calculations at CAM-B3LYP/6-311++G (d,p). Also, the contributing configurations and MOs are characterized by the origin of each absorption band. The charge transfer of the electron density in the studied compounds is characterized by Natural Bond Orbital analysis (NBO). Due to theoretical chemistry, it has become possible to anticipate many physical and chemical properties of molecules. In the current examination, using DFT calculations, structural entities, chemical reactivity parameters, spectroscopic data, some global reactivity descriptors have been explored. The spectrophotometric measurements of elucidating the optical constants of the prepared compounds **1–4** are investigated in a wide range of spectra. This is the framework for our previous work (Abdel Halim and Ibrahim 2019; Abdel Halim et al. 2017; Abdel Halim and Ali, 2017) which aims to study the properties of compounds **1–4** and predict their applications. We provide a broad description of the chemical reactivity of compounds **1–4** from the analysis of the natural bond orbital (NBO), DFT method was implemented of molecules were explored as well. The molecular modeling study with a hybrid quantum mechanical on this titled compound is not available. The structure and binding properties are new perceptions for this study. In addition, the potential molecular electrostatic (MEP) and UV–visible analyses were studied using theoretical calculations and experimental to provide spectra and structure electronic of compounds **1–4** using CAM-B3LYP/6-311++G (d,p), information on the charge transfer within each molecule. All calculations in this research have been done by using to DFT method at the B3LYP/6-311++G (d, P) theory level.

2 Experimental

2.1 Solvents

Polar (Methanol and Butanol) and non-polar (Dioxane and Toluene) solvents were obtained from Merck, AR- grade, and were used without further purification.

2.2 Apparatus

A Perkin Elmer lambda 4B spectrophotometer using 1.0 cm fused quartz cells were used to measure the electronic absorption spectra over the range 200–900 nm. Spectral analysis of transmittance and reflectance are performed in the wavelength range of 200–750 nm.

2.3 Antimicrobial study

Biological activities of synthesized compounds **1–4** were studied for antibacterial and antifungal properties against different types of bacteria; Gram-positive- *S*. aureus, and *B. subtilis* and Gram-negative- *S. Typhimurium* and *E. Coli* also; *Yeast -C. albicans* for fungus. *A. fumigatus*.

2.4 Computational details

Khon-Sham's (DFT) calculations were performed on an Intel (R) Core (TM) i7 computer using Gaussian-09 program package without any constraint on the geometry. [36] The geometry of the molecules studied in this is optimized by DFT/B3LYP method using 6-311++G (d, p) basis set (GaussView 2009). The FMO analysis and quantum chemical study has been performed using GaussView 5.0.9 or chemcraft 1.6 software packages (Avci 2011). Also, the following equations, were calculated the total static dipole moment (μ), $\langle \Delta \alpha \rangle$, and $\langle \beta \rangle$, values (Avci et al. 2010).

$$\mu = (\mu_x^2 + \mu_y^2 + \mu_z^2)^{1/2},$$
$$\langle \alpha \rangle = 1/3(\alpha_{xx} + \alpha_{yy} + \alpha_{zz}),$$
$$\Delta \alpha = \left(\left(\alpha_{xx} - \alpha_{yy}\right)^2 + \left(\alpha_{yy} - \alpha_{zz}\right)^2 + \left(\alpha_{zz} - \alpha_{xx}\right)^2 /2 \right)^{1/2}, \quad (1)$$
$$\langle \beta \rangle = \left(\beta^2 x + \beta^2 y + \beta^2 z \right)^{1/2},$$

where

$$\beta_x = \beta_{xxx} + \beta_{xyy} + \beta_{xzz},$$
$$\beta_y = \beta_{yyy} + \beta_{xxy} + \beta_{yzz}, \quad (2)$$
$$\beta_z = \beta_{zzz} + \beta_{xxz} + \beta_{yyz}.$$

Using the predicted energies of HOMO and LUMO, global reactivity descriptors were calculated as follows: $\chi = (I + A)/2$ (electronegativity), $\eta = (I - A)/2$ (chemical hardness), $S = 1/2\eta$ (global softness), $\omega = \mu^2/2\eta$ (electrophilicity) where *I* and *A* were
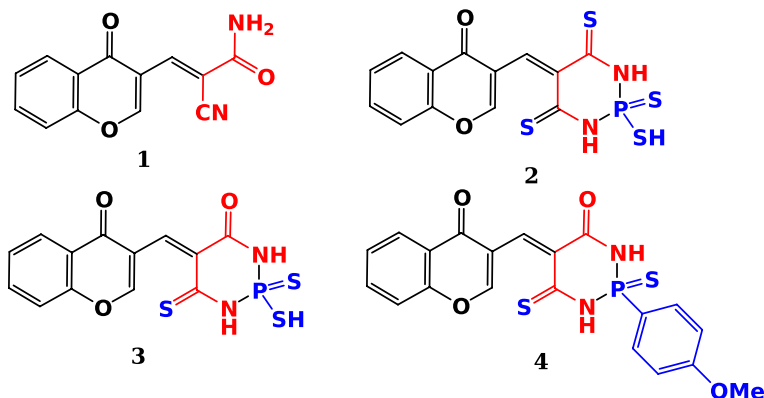
Scheme 1 Schematic representation of the compounds **(1–4)**

ionization potential and electron affinity, and $I = -E_{HOMO}$ and $A = -E_{LUMO}$, respectively (Matecki, 2010). Absorption energies (λ in nm), Oscillator strength (*f*), and transitions of all compounds **1–4** have been calculated at TD-CAM -B3LYP/6-311++G (d, p) level of theory (Yanai et al. 2004).

The natural bond orbital method (NBO) used to investigate the reactive sites of the compounds **1–4**, the molecular electrostatic potential (MEP) was computed, the donor–acceptor interactions was used to evaluate the second order Fock matrix (Yanai et al. 2004; Szafran et al. 2007). For each donor (*i*) and acceptor (*j*), the stabilization energy $E^{(2)}$ associated with the delocalization $i \rightarrow j$ was estimated as:

$$E^{(2)} = \Delta E_{ij} = q_i \left(F(ij)^2 / \varepsilon_j - \varepsilon_i \right), \tag{3}$$

where q_i is the donor orbital occupancy, ε_i and ε_j are diagonal elements and $F(ij)$ is the off-diagonal NBO Fock matrix element. For the conversion factors of α, β, and HOMO and LUMO energies in atomic and cgs units: 1 atomic unit (a.u.) = 0.1482×10^{-24} electrostatic unit (esu) for polarizability ⟨α⟩; 1 a.u. = 8.6393×10^{-33} esu for first hyperpolarizability ⟨β⟩.

3 Result and discussion

3.1 The studied compounds

The studied compounds were prepared and reported in the literature (Frisch et al., 2009). The proposed compounds **1–4** is shown in Scheme 1. They are 2-cyano-3-(4-oxo-4*H*-chromone-3-yl)prop-2-enamide (**1**), 5-[(4-oxo-4*H*-chromen-3-yl)methylidene]-4,6-dithioxo-2-sulfanyl-2-sulfido-1,3,2-diazaphosphinane (**2**), 5-[(4-oxo-4*H*-chromen-3-yl)methylidene]-2-sulfanyl-2-sulfido-6-thioxo-1,3,2 diazaphosphinan-4-one (**3**) and 2-(4-methoxyphenyl)   -5-[(4-oxo-4*H*-chromen-3-yl)methylidene]-2-sulfido-6-thioxo-1,3,2-diazaphosphinan-4-one (**4**).
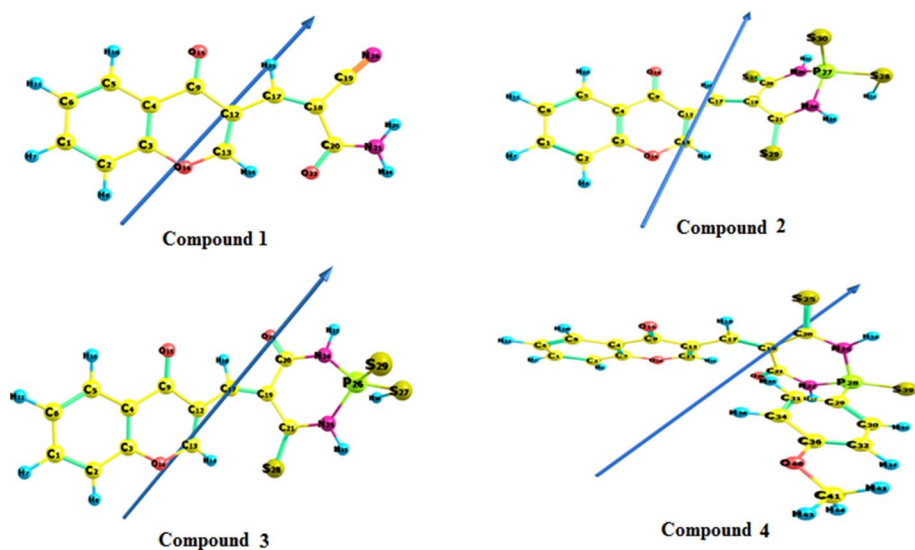
Fig. 1 The optimized structure, perspective view of dipole moment of the compounds **1–4** at B3LYP/6-311++G (d, p)

Table 1 Total energy, energy of HOMO and LUMO, energy gap, dipole moment, The ionization potential (**I** /eV), electron affinity (**A** /eV), chemical hardness η/ eV), global softness (**S**/eV^{-1}), chemical potential (*V/eV^{-1}*), electronegativity (χ/eV), and global electrophilicity index, (ω/eV), of the compounds **1–4** computed at the B3LYP/6-311++G(d,p)

Compounds	1	2	3	4
E_T (au)	− 835.5737	− 2695.2023	− 2372.2494	− 2319.6968
E_{HOMO} (eV)	−6.90118	−6.46681	−6.64006	6.14366
E_{LUMO} (eV)	−2.69661	−3.06843	−3.05402	2.80133
E_{gap} (eV)	4.20457	3.39837	3.58604	3.34233
μ (Debye)	5.0714	4.0698	4.2418	7.4535
I (eV)	6.90118	6.46681	6.64006	6.14366
A(eV)	2.69661	3.06843	3.05402	2.80133
X(eV)	4.79889	4.76762	4.84704	4.47249
V(eV^{-1})	− 4.79889	− 4.76762	− 4.84704	− 4.47249
η(eV)	2.10229	1.69918	1.79302	1.67116
S(eV^{-1})	0.23784	0.29426	0.27886	0.29919
ω (eV)	1.20616	1.19757	1.18286	2.23003

3.2 Electronic structures

3.2.1 Geometry, ground state properties and global reactivity descriptors

Figure 1 and Table 1 described all compounds **1–4** have been studied using density functional theory DFT/B3LYB at 6-311++G (d,p) basis set to determine various structural and chemical parameters. The compound **4** has the highest polarity (μ = 7.4535 Debye) whereas the compound **2** has the lowest polarity (μ = 4.0698 Debye) amongst 1,3,2-diazaphosphinines. This can be clarified by considering Fig. 1. In case of compound **4**, 2-(4-methoxyphenyl) having opposite electronic effect are present at the two termini which lead to

augmentation in polarity of the molecules. However, in case of compound **2**, (2-sulfanyl) exactly opposite situation is present thereby results in decrease of polarity, and hence the order **4 > 1 > 3 > 2** (c.f. Table 1) in addition to the vector of the dipole moment was presented in Fig. 1. The phenomenon of the polarity is extremely crucial to foresee which compounds would enter through the lipophilic membrane of the microorganisms.

The optimized geometrical parameters (bond lengths and bond angles) were shown in Figs. S1 and S2. All compounds **1–4** is having C1 point group symmetry as predicted by DFT investigation. The calculated bond lengths of C_1-C_2, C_2-C_3, C_3-C_4 and C_4-C_5 in the benzo rings of the chromone moiety were in the range from 1.387 to 1.509 Å in all the studied compounds **1–4** (c.f. Fig. S1). These were overestimated than the experimental values by 1%, whereas the computed C-P and C-S bond lengths are overestimated than the experimental values by 4%. At the same time, the computed geometry of the bond lengths of the compounds **1–4** were found in between (1.449 and 1.479 Å) which like bond length in the literature (Sajan et al. 2011a), also; small difference in geometry of the bond angles for studied compounds (c.f. Fig. S2), this caused by the method of calculation which was carried out in gas phase and observed in solid state. The frontier molecular orbital's (FMO) of previously synthesized compounds **1–4** is presented in Figs. 2 and 3 the electronic parameters and the global reactivity descriptors' statistics are given in Table 1. All the compounds are non-planner as reflected from their dihedral angles. The dihedral angles and natural charge of the studied compounds **1–4** were listed in Table 2. In the parent compound **1**, the planarity changed by the presence of the phosphorus and sulfur atoms in diazaphosphinanes rings, by the range from 11 to 125°. So, there is no planarity for all compounds **2–4** as indicated from the dihedral angles (c.f. Table 2).

The FMO study indicates that the compound **4** has the lowest energy gap (3.3423 eV) and on the other hand the compound **1** possesses the highest energy gap (4.2046 eV). The lower HOMO–LUMO energy gap in the compound **4** demonstrates the inevitable charge transfer is happening within the molecule and it is easier as compared with the other compounds **1–3**. Amongst all compound **1–4**, compound **4** has more reactive HOMO (E = −6.1437 eV) and compound **1** has less reactive HOMO (E = −6.9012 eV). The LUMO with least energy is present in the compound **4** (E = −2.8013 eV) and with high energy in the compound **1** (E = −2.6966 eV). The molecule with the highest

Fig. 2 Energy of HOMO, LUMO and energy gap of the studied compounds **1–4** at B3LYP/6-311++G (d, p) level of theory
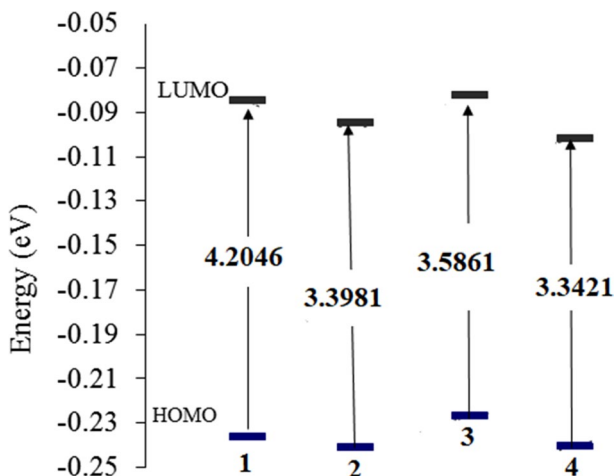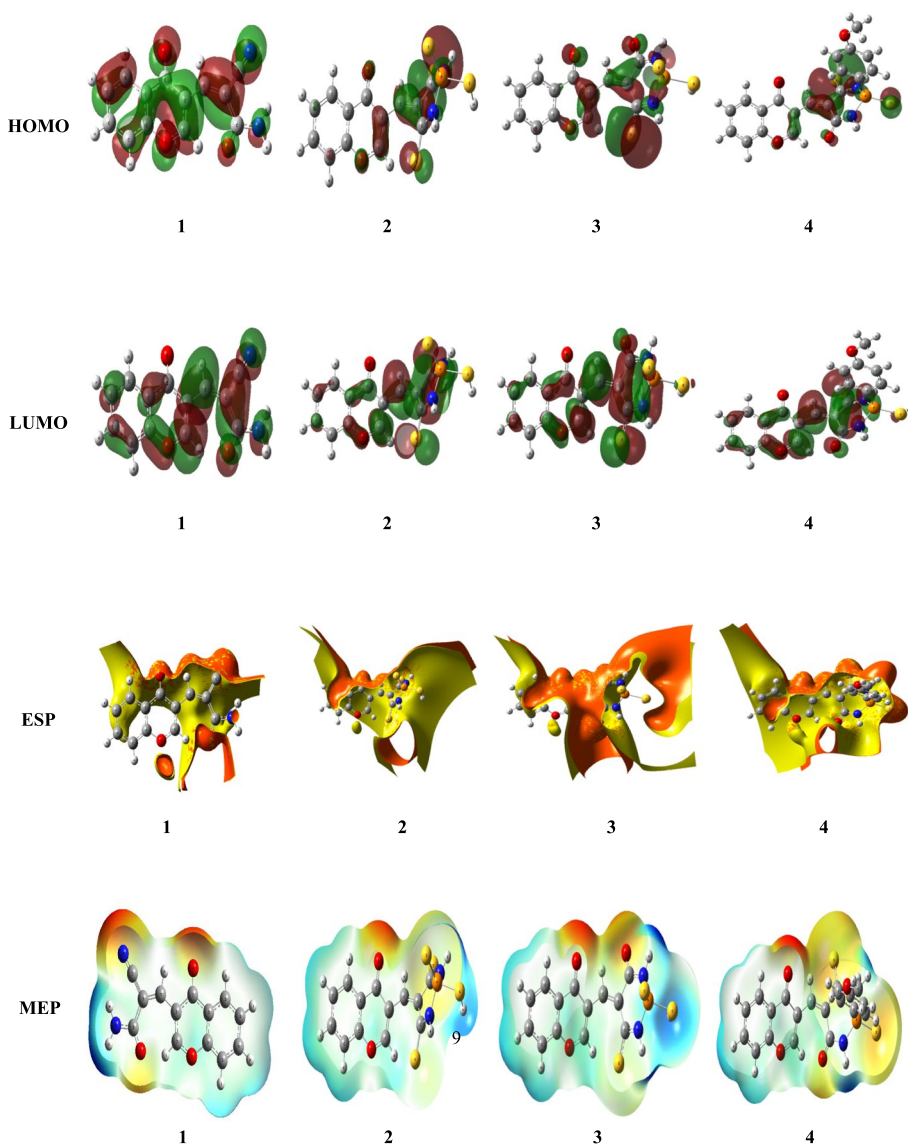
Fig. 3 HOMO, LUMO and Molecular surfaces of compounds **1–4** at B3LYP/6-311++G (d,p)

ionization potential is compound **1** (E=6.9012 eV) and with the lowest value is compound **4** (E=6.1437 eV). The electron affinity value is higher for the compound **4** (E=2.8013 eV) and is lower for the compound **1** (E=2.6966 eV). In brief, the two compound **1** and compound **4** are having exactly opposite electronic and chemical behavior.

The global descriptor study suggests all these are good electrophiles as the value of global electrophilicity (ω) is less than the other parameters ((η), (**S**), (**V**), (χ)). As far as global softness is concerned the compound **4** is the softest among all compound **1–3** with a global softness value of 0.2992 eV. The absolute hardness is higher for the compound **1**

Table 2 Natural Charge for the studied compounds **1–4** computed at the B3LYP/6–311++G(d,p) level of theory

Parameters	1	2	3	4
Natural charge				
O15	− 0.58608	− 0.57582	− 0.57552	− 0.58174
O16	− 0.45600	-0.45925	− 0.45801	− 0.45822
O22	− 0.65316	–	− 0.57548	− 0.61486
N21	− 0.77842	− 0.92758	− 0.97986	− 0.91106
N24	− 0.33129	-0.92228	− 0.92201	− 0.95589
O25	–	–	–	–
O26	–	–	–	–
P27	–	1.40775	1.42067	1.63626
S24	–	− 0.07315	− 0.23654	− 0.10806
S28	–	− 0.23226	− 0.12196	–
S29	–	− 0.10375	− 0.46314	–
S30	–	− 0.44482	–	–

For numbering system, see Fig. 1

and it is 2.1023 eV. The ease of removal of an electron is governed by its chemical potential V (eV) and it is likewise identified with its electronegativity. A good electrophile is described by a higher value of global electrophilicity (ω) and the lower value of ω indicates good nucleophile. Our results suggest that the compound **4** ($\omega = 2.2300$ eV) has a higher value of ω, so it is most likely to accept electrons readily and would undergo nucleophilic attack easily. On the other hand, the compound **3** ($\omega = 1.1829$) has a lower electrophilicity indicating that it is a potent nucleophile or can lose easily. As V value increases, the ability of a molecule to lose an electron increase.

3.3 Natural charge

The natural population analysis was performed on the electronic structures of compounds **1–4** are calculated by DFT/B3LYP method with 6-311++G (d, p) basis set in the gaseous phase are given in Table 2 and indicated by colors in Fig. 4, it is clearly described the distribution of electrons in various sub-shells of their atomic orbits (Reed et al. 1985). Natural atomic charges reveal that all the phosphor (P27) atoms have a net positive charge but in the compound **4** has a more positive charge (1.63626) than other compound **1–3**. The high positive character is due to the attachment with a nitrogen atom and Sulphur atom. Amongst the oxygen atom (O22) and the nitrogen atom (N24), have a more negative charge, and the value is − 0.65316 and − 0.95589 respectively.

3.4 Atomic charge distribution

3.4.1 Polarizability and hyperpolarizability

The relationship between the molecular structure and NLO phenomena for the compounds **1–4** were calculated using DFT/B3LYP/6-311++G (d,p) has been also theoretically obtained (Natorajan et al. 2008). Table 3 shows that the mean first order hyperpolarizability $\langle \beta \rangle$ (Octapole moment), total static dipole moment (μ), the mean polarizability ($\langle \alpha \rangle$)

Atomic charge distribution

□ Negative Charge value
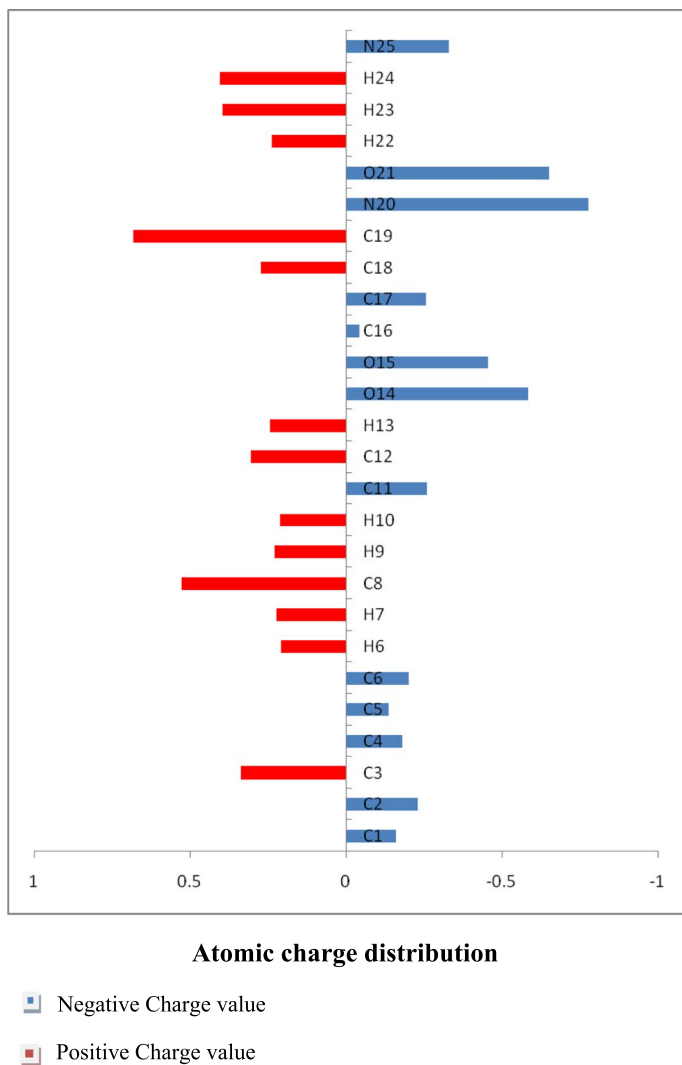
■ Positive Charge value

Fig. 4 Atomic charge distribution (au) for compound **1** at B3LYP/6-311++G (d,p) basis set

(Quadrupole moment), and the anisotropy of the polarizability ($\Delta\alpha$), of the compounds **1–4**. The calculated high value of dipole moment was found to be 7.4535 D for compound **4** than the other compounds **1–3** at B3LYP/6-311++G (d,p). Also; the calculated mean polarizability ('α') is 66.33×10^{-24} esu i.e. two times higher than p-nitroaniline (PNA) molecule, the order of increasing α with respect to PNA was showed in Table 3 that values of α, β: compounds **3**, **2** and **4** are ~ 2.5 and 3 times higher than PNA, whereas compounds **1** are ~ 1.5 times higher than the standard PNA, respectively. In addition, the calculated mean first order hyperpolarizability $\langle\beta\rangle$, of the compound **4** is 74.87×10^{-30} esu and compound **3** is 58.65×10^{-30} esu i.e., higher than PNA molecule (Table 3), while compounds **1, 2** are ~ 1.5, and 2.5 times higher than the reference respectively. Obtained value indicates that the studied compounds **1–4** might be a promising NLO material. Due to the lack of any

Table 3 Total static dipole moment (μ), the mean polarizability ($\langle\alpha\rangle$), the anisotropy of the polarizability ($\Delta\alpha$), and the mean first-order hyperpolarizability ($\langle\beta\rangle$), for the compounds **1–4** computed at B3LYP/6–311++G(d,P)

Property	p-nitroaniline (PNA)	1	2	3	4
μ_x, D	2.44	-3.3164	2.4466	3.0322	1.2791
μ_y, D		-3.8367	3.2335	2.9240	6.5552
μ_z, D		0.0008	-0.3492	-0.4988	-3.3088
μ, Debye[a]		5.0714	4.0698	4.2418	7.4535
α_{XX}, a.u		-80.9781	-123.8534	-119.4947	-143.6198
α_{XY}, a.u		-12.1868	-0.2942	-0.3290	-17.3575
α_{YY}, a.u		-112.4434	-173.3651	-164.8106	-188.0664
α_{ZZ}, a.u		-104.1046	-175.2720	-165.0014	-201.4035
α_{YZ}, a.u		-0.0006	-2.2414	-2.2841	0.4286
α_{XZ}, a.u		-0.0025	10.6021	15.5762	-8.4368
$\langle\alpha\rangle \times 10^{-24}$esu[b]	22	34.70	53.34	42.19	66.33
$\Delta\alpha \times 10^{-24}$esu		41.84	74.83	67.30	77.66
βxxx, a.u		-57.5795	171.7577	213.5309	142.1719
βxxy, a.u		-99.2777	37.5040	24.0534	233.7926
βxyy, a.u		-36.2411	10.1630	11.9290	-32.0003
βyyy, a.u		-41.5084	13.2984	-3.1938	133.6417
βxxz, a.u		-0.0070	1.6036	-17.8477	-43.9200
βxyz, a.u		-0.0059	-6.7244	-10.0682	19.7077
βyyz, a.u		0.0049	-0.0023	8.2361	-7.3963
βxzz, a.u		11.0241	32.6290	8.8481	4.3800
βyzz, a.u		-2.9331	9.1021	13.5789	24.5709
βzzz, a.u		-0.0052	2.0979	-9.9996	-45.8107
$\langle\beta\rangle \times 10^{-30}$esu[c]	15.5	37.54	45.23	58.65	74.87

[a, b, c] *p*-nitroaniline (PNA) results are taken from references (Stadler et al. 1995; Kaatz et al., 1998; Gnanasambandan et al. 2014)

experimental NLO data about the examined compound, PNA, that is one of the typical NLO structure was chosen as reference material (Stadler et al. 1995; Kaatz et al. 1998; Gnanasambandan et al. 2014).

3.4.2 Molecular electrostatic potential (MEP)

The MEP plots for the studied compounds **1–4** are presented in Figs. 3 and 4. The MEP plots suggest that the chromone ring attached to the 1,3,2-diazaphosphinines ring is highly susceptible to electrophilic aromatic substitution. In all the studied compounds **1–4**, the blue part is situated at the NH group suggesting high reactivity towards basic reagents and caused by while the positive (blue) potential sites were around the hydrogen, and carbon atoms. Blue for electron deficient, (partially positive charge); light blue for (slightly electron deficient region); yellow for (slightly electron rich region); green for neutral (zero potential) respectively (Sajan et al. 2011b).

3.5 Electronic UV-spectra

Absorption energies (λ in nm), oscillator strength (f), and transitions of all studied compounds **1–4** have been computed at TD-DFT-CAM-B3LYP/6-311++G (d,p) level of theory for optimized geometries.

The results of the TD-DFT were carried out in both the gas phase and in polar solvent (methanol and butanol) and non-polar solvent (dioxane, and toluene) for the low intensity bands (Q-region) and high-intensity bands of the compounds **1–4** to understand the electronic transitions of the compounds **1–4**. Compounds 1–4's electronic spectra in methanol and butanol solvents, as well as spectrum assignment, are shown in Figs. S3-S10 and Tables S1-S4.

The effect of the solvent clear in transition from a non-polar to a polar solvent and increasing solvent polarity causes small changes in band positions; the intensity of all bands is assigned to (π-π*) and (n-π*) transitions as reflected by their intensities (0–110,000), which results from electron excitation of the highest occupied molecular orbitals and the lowest vacant molecular orbitals.

The first (n-π*)^1 state is centered at (430 nm) in non-polar solvents (dioxane, and toluene) respectively, this band is predicted theoretically at (450 nm) (state 9), respectively is very good agreement with the experiment. The gas phase calculation gave a wavelength at 420 nm. Moreover, in polar solvents (methanol and butanol), this same band appeared at (411 nm) respectively, where theoretical calculations in (methanol and butanol), reproduced this band at (425 nm) (state 11), as shown in Table S1. The electron density contours of molecular orbital's nature indicted by the electronic transition. The ten orbital's $\varphi_{59-68}{}^{-1}$ involved in the theoretical transitions of compound **1**, is shown in Fig. S11, showed a delocalization of electron density, and charge transfer CT character. From second state to eight states, the same desiccation as well as the first state is shown in c.f. (Figure S11.) and Table S1). These absorption bands in the visible region are typical n-π*, π–π* transitions. The absorption band that corresponds to the maximum absorption of the compound **1**, is blue and red shifted by 3–4 nm under the effect of solvent. For comparison, Table S2 contains the theoretical and the experimental vertical excitation energies and the corresponding oscillator strengths for compound **1**.

The first (n-π*)^1 state in compounds **2–4** are centered at (450 nm) in non-polar solvents (dioxane, and toluene) respectively, this band is predicted theoretically at (500 nm) (state 9), respectively is very good agreement with the experiment. The gas phase calculation gave a wavelength at 460 nm. Moreover, in polar solvents (methanol and butanol), this same band appeared at (450 nm) respectively, where theoretical calculations in (methanol and butanol), reproduced this band at (480 nm) (state 11), as shown in Tables S2–S4. The electron density contours of molecular orbital's nature indicted by the electronic transition. The ten orbital's $\varphi_{87-103}{}^{-1}$, $\varphi_{85-97}{}^{-1}$ and $\varphi_{102-116}{}^{-1}$, respectively involved in the theoretical transitions of compounds **2–4**, is shown in Fig. S11, showed a delocalization of electron density, and charge transfer CT character. From second state to eight states, the same desiccation as well as the first state (c.f. Tables S2–S4). These absorption bands in the visible region are typical n-π*, π–π* transitions. The absorption band that corresponds to the maximum absorption of the compounds **2–4**, is blue and red shifted by 3–4 nm under the effect of solvent. For comparison, Tables S2–S4 contains the theoretical and the experimental vertical excitation energies and the corresponding oscillator strengths for compounds **2–4**.

Table 4 presented the second order perturbation energies of most interacting NBOs of **1–4** and the most important interaction between filled (donor) Lewis's type

Table 4 Second Order Perturbation Interaction Energy Values Computed in the NBO Basis for the compounds **1–4**, calculated at B3LYP/6-311++G (d,p)

Compound	Donor	Acceptor	$E^{(2)a}$(kcal/mol)	NBO	Population
1	πC1–C2	π*C3–C4	22.54	πC1–C2	1.68405
	πC12–C13	π*C9–O15	23.03	C12–C13	1.74546
	πC17–C18	π*C19–N26	22.17	C17–C18	1.81156
	LP (1) O22	RY*C20	14.39	LP (1) O22	1.96996
	LP (2) O16	σ*C12–C13	36.17	LP (2) O16	1.71837
	LP (1) N21	π*C20–O22	64.83	LP (1) N21	1.72548
	LP (2) O22	π*C20–N21	22.76	LP (2) O22	1.86540
	LP (1) N26	RY*C19	16.95	LP (1) N26	1.96790
	LP (1) N26	σ*C18–C19	12.03	C3–C4	0.41489
	π*C3–C4	π*C5–C6	176.33	C20–O22	0.33407
	π*C20–O22	π*C17–C18	106.80	C17–C18	0.17455
	π*C17–C18	π*C19–N26	12.27		
2	πC4–C5	π*C2–C3	26.29	C4–C5	1.60039
	πC12–C13	π*C9–O15	21.71	C12–C13	1.76214
	πC17–C19	π*C21–S29	19.54	C17–C19	1.77191
	LP (2) O16	π*C12–C13	35.11	LP (2) O16	1.72526
	LP (2) S24	π*C19–C20	10.24	LP (2) S24	1.87410
	LP (1) N26	π*C21–S29	44.44	LP (1) N26	1.70605
	LP (2) S29	π*C21–N26	12.90	LP (2) S29	1.88008
	LP (2) S30	π*P27–S28	20.43	LP (2) S30	1.74396
	LP (3) S30	π*P27–N25	16.56	LP (3) S30	1.71291
	π*C2–C3	π*C1–C6	299.26	C2–C3	0.39013
	σ*C20–S24	σ*C17–C19	23.45	C20–S24	0.29784
	σ*C20–S24	σ*C20–S24	20.69	P27–N25	0.23420
	σ*P27–N25	RY*P27	10.16		
	σ*P27–N25	σ*P27–S30	26.69		
3	πC17–C19	π*C21–S28	22.76	C17–C19	1.77242
	LP (1) N24	σ*C20–O31	32.51	LP (1) N24	1.76264
	LP (1) N25	π*C21–S28	47.52	LP (1) N25	1.70598
	π*C3–C4	π*C5–C6	171.85	C3–C4	0.41489
	π*C17–C19	π*C20–O31	64.39	C20–O31	0.24315
	σ*C21–S28	σ*C17–C19	18.53	C21–S28	0.36331
	σ*P26–N24	RY*P26	11.20	P26–N24	0.21626
	σ*P26–N25	σ*P26–N24	15.14	P26–N25	0.23190
	σ*P26–N25	σ*P26—S29	30.80		
4	LP (2) O24	π*C21–N27	25.43	LP (2) O24	1.86046
	LP (1) N26	π*C20–S25	40.76	LP (1) N26	1.69872
	LP (2) S39	π*P28C29	13.35	LP (2) S39	1.81836
	LP (2) O40	π*C32–C36	33.49	LP (2) O40	1.82351
	π*C2–C3	π*C1–C6	315.64	C2–C3	0.39035
	π*C21–O24	π*C17–C19	51.69	C21–O24	0.28123

[a]$E^{(2)}$ means energy of hyperconjugative interactions (stabilization energy)

LP$_{(n)}$ is a valence lone pair orbital (n) on atom

NBOs and empty (acceptor) non-Lewis NBOs. Figure S11 presented the charge density maps of HOMO and LUMO for **1–4**. The results of NBO analysis of compound **1** were tabulated in Table 4 indicated that there was a strong hyper conjugative interactions π^*C_3–$C_4 \rightarrow \pi^*C_5$–C_6, π^*C_{20}–$O_{22} \rightarrow \pi^*C_{17}$–$C_{18}$, LP (1) $N_{21} \rightarrow \pi^*C_{20}$–$O_{22}$, and LP (2) $O_{16} \rightarrow \sigma^*C_{12}$–$C_{13}$, for compound **1** was 176.33, 106.80, 64.83, and 36.17 kcal/mol, respectively. The C–O π orbital and quinoline ring interacted equally well with chromone ring. It was surprising to notice a decrease in the population of the NBO C_1–C_2, and C_3–C_4 reflecting a charge transfer away from the chromone ring. In conclusion, compound **1** enjoyed the linear conjugation for the observed spectrum. For compound **2** showing hyper conjugative strongly interactions π^*C_2–$C_3 \rightarrow \pi^*C_1$–C_6, and LP (1) $N_{26} \rightarrow \pi^*C_{21}$–$S_{29}$, for **2** was 299.26 and 44.44 kcal/mol, respectively. NBO analysis of the compound **2** in Table 4 indicated that it retained the extended conjugation of **1** as revealed by the interaction of C–O NBOs with those of chromone ring. Furthermore, the oxygen lone pair orbital and nitrogen atoms enjoyed hyperconjugation with the C_{21}–S_{29}, and C_{12}–$C_{13}\pi^*$ orbital. It was surprising to notice a decrease in the population of the NBO P_{27}–N_{25}, C_{20}–S_{24}, and C_2–C_3 reflecting a charge transfer away from the chromone ring. There was a strong hyper conjugative interaction in Compound **3** π^*C_3–$C_4 \rightarrow \pi^*C_5$–C_6, π^*C_{17}–$C_{19} \rightarrow \pi^*C_{20}$–$O_{31}$ and LP (1) $N_{25} \rightarrow \pi^*C_{21}$–$S_{28}$, for **7** is 171.85, 64.39 and 47.52 kcal/mol, respectively. Furthermore, the lone pair orbital of the oxygen and nitrogen atoms enjoyed hyperconjugation with the C_5–C_6, and C_{17}–C_{19} π*-orbital. The population of the NBO P_{26}–N_{24}, P_{26}–N_{25}, C_{20}–O_{31}, C_{21}–S_{28} and C_3–C_4 decrease surprising and reflecting a charge transfer away from the chromone ring. This was also evident in the case of the population of the oxygen lone orbital LP (1) N_{25}. The results of compound **4** of NBO analysis tabulated in Table 8 indicated that there was a strong hyper conjugative interactions π^*C_2–$C_3 \rightarrow \pi^*C_1$–C_6, π^*C_{21}–$O_{24} \rightarrow \pi^*C_{17}$–$C_{19}$, and LP (1) $N_{26} \rightarrow \pi^*C_{20}$–$S_{25}$, for **4** was 315.64, 51.69 and 40.76 kcal/mol, respectively. There is the extended conjugation of **1** with the compound **4** as revealed by the interaction of C–O NBOs with those of chromone ring. Furthermore, the lone pair orbital of the oxygen and nitrogen atoms enjoyed hyperconjugation with the C_{17}–C_{19}, C_1–C_6 and C_{20}–S_{25} π* orbital. It a decrease in the population of the NBO C_{21}–O_{24}, and C_2–C_3 reflecting a charge transfer away from the chromone ring can be surprised. This was also evident in the case of the population of the oxygen lone orbital LP (1) N_{26}.

3.6 Optical band gap of the presented structures

The optical energy gap (Eg) of the compounds **1–4** can be determined experimentally by the Eq. (1) (Hemalatha et al. 2014):

$$(\alpha E)^2 = A(E - E_g) \tag{4}$$

where E is the incident photon energy and A is a constant. Figure S12 shows; the values of E_g for every structure that resulting from $[(\alpha E)^2 \, vs. (E)]$ plots can be extracted from extrapolation of linear parts of the curve for each case to $(\alpha \, hv)^2 = 0$, and the best fit of most feasible transition supports the direct band transition.

3.7 Antimicrobial activity

The biological activities of synthesized compounds **1–4** was investigated for antibacterial and antifungal characteristics against various bacteria, including Gram-positive S. aureus and B. subtilis, as well as Gram-negative *S. Typhimurium* and *E. Coli*, and yeast, C. albicans. A. fumigatus is a species of A. fumigatus. Measuring the growth inhibition (zone of inhibition) around the disc of material that has been recorded. The findings are shown in Table 5 and Fig. 5. Antibiotics' antibacterial efficacy was evaluated, and the results revealed that they were ineffective against all bacteria and fungus. The tiny size of compound **4** improves its absorption capacity on the surface of the cell wall of microorganisms and the respiration process of the cell, which explains the strong antibacterial activity against all tested bacteria and fungi. As a result, compound **4** is required for the growth-inhibitor effect to occur.

3.8 Structure activity relationship (SAR)

The computed ground state energetic and global characteristics can be linked to the biological activity of the produced molecules **1–4**. The biological activity of the investigated compound (**1–4**) produced experimentally follows the sequence **4 > 1 > 3 > 2** against G+, G−, and fungi, as shown in (Table 1 and 5). The energy gap, Eg, of the studied compound computed at B3LYP/6-311++G (d,p) follows the same order obtained experimentally, indicating that Eg is one of the factors contributing to the reactivity of the studied compounds, E_{HOMO}, which measures the donating power, the order of E_{HOMO} **4 > 1 > 3 > 2**, and dipole moment, which measures the polarity (c.f. Table 1). The investigated compounds theoretically calculated global softness (S), global electrophilicity index (ω), electronegativity (χ), and chemical potential (V) follow the same sequence as their experimental biological activity, which is **4 > 1 > 3 > 2**. The chemical hardness (ɳ) follows the experimental biological activity in reverse order: **4 < 1 < 3 < 2**. The order of natural charge from NBO and mean first-order hyperpolarizability (β) is **4 > 1 > 3 > 2**, which is contrary to the order of experimental biological activity. Finally, the substituent in compounds **1–4** boosts the biological activity of the molecule.

4 Conclusion

In summary, we have explored various facets of the electronic structure of 1,2,3-diazaphosphinanes bearing a chromone ring for all studied compounds **1–4**, were investigated theoretically by using DFT method at B3LYP/6-311++G (d, p) and TD-DFT at CAM/B3LYP/6-311++G (d, p) level theory. All these molecules possess C1 point group symmetry. For a detailed structural analysis, the optimized geometrical parameters like bond lengths and bond angles have been discussed, also all compounds were found to be non-planar structure indicated by dihedral angle. Frontier molecular orbital analysis of all compounds **1–4** has been computed and the results indicate that the compound **4** had the lowest E_{HOMO}, E_{LUMO}, and E_{gap} indicating highest reactivity amongst all compounds. This means that the charge transfer is easier in compound **4** than other compounds. Various quantum chemical parameters have been computed to analyze the chemical nature of the molecules. The neutral atomic charges for all compounds **1–4** which indicated the

Table 5 In vitro antimicrobial activities of the synthesized compounds at 500 and 1000 μg/mL and the MIC values for some selected compounds

Compound	Conc. (μg/ml)	Zone of inhibition in mm* and (MIC values in μg/mL)					
		Bacteria Gram (+) ve		Bacteria Gram (-) ve		Yeast	Fungi
		S. aureus	*C. albicans*	*S. typhimurium*	*E. coli*	*C. albicans*	*A. fumigatus*
1	500	–	–	–	–	14 (250)	–
	1000	–	–	–	–	20	–
2	500	–	–	–	–	10	–
	1000	–	–	–	–	15	–
3	500	–	–	–	–	13 (249)	–
	1000	–	–	–	–	19	–
4	500	–	–	–	–	12	–
	1000	–	–	–	–	16	–
S**	500	26	25	28	27	28	26
	1000	35	35	36	38	35	37

*Low active: 6–12 mm; moderately active: 13–19 mm; highly active: 20–30 mm; –: No inhibition or inhibition less than 5 mm

S**: Standard drugs
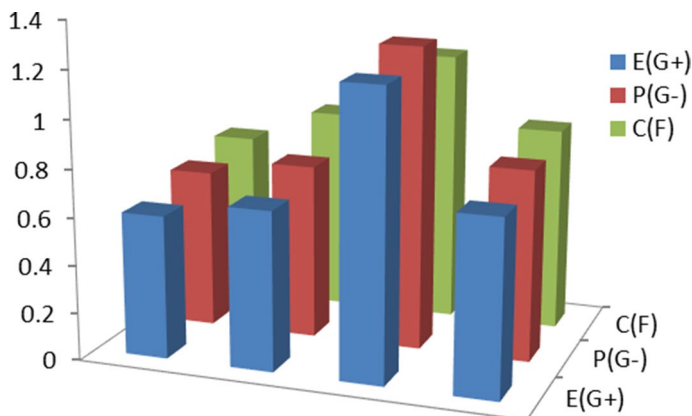
Fig. 5 Antimicrobial activity for the studied compounds **1–4** against gram-positive bacteria (G$^+$), gram-negative bacteria (G$^-$), and Fungi (F)

electronic charge distribution have been discussed. The calculated dipole moment and first order hyperpolarizability results indicated that the molecule had a reasonably good nonlinear optical behavior. The molecular electrostatic potential (MEP) surfaces are plotted to point out the electrophilic and nucleophilic reactivity sites. UV spectra have been computed at TD-DFT-CAM/B3LYP/6-311++G (d, p) level of theory of the compounds **1–4**. All the observed bands can be assigned to (n-π*, π–π*) transitions as reflected from their intensities. The correspondence between the theoretically computed and the experimentally observed transitions are satisfactory. The solvent dependence of the observed bands can be attributed to the charge in the dipole moments of the ground and excited states. The NBO analysis of the compounds **1–4** indicated the intermolecular charge transfer between the bonding and anti-bonding orbitals. Band gaps optical were extracted from the photon energy dependence on absorption coefficient at the band edges and found to be 2.94, 2.65, 2.70 and to 2.92 eV, respectively. In this way, we can conclude that the information furnished in this research could provide ladder for the development of further research in the respective fields. Theoretically, the reactivity of the studied compounds follows the order: **4 > 1 > 3 > 2** which is the same order of reactivity towards G−, G+ and fungus.

Data availability All data available.

Declarations

Competing interest The authors declare that they have no known competing financial interest or personal relationships that could have appeared to influence the work reported in this paper.

Consent for publication This manuscript is original, has been written by the stated authors who are all aware of its content and approve its submission.

Ethical approval The authors comply with ethical standard in this paper writing.

References

Abdel Halim, S., Ibrahim, M.A.: Density functional theory band structure calculations, optical, and photoelectrical characterizations of the novel (9-Bromo-3-cyano-5-oxo-1,5-dihydro-2H-chromeno[4,3-b] pyridin-2 ylidene) propanedinitr. J. Heterocycl. Chem. **56**, 2542–2554 (2019)

Abdel Halim, S., Khalil, A.K.: TD-DFT calculations, NBO analysis and electronic absorption spectra of some thiazolo[3,2-a] pyridine derivatives. J. Mol. Struct. **1147**, 651–667 (2017)

Abdel Halim, S., Ali, L.I., Sanad, S.G.: Theoretical calculations of solvation 12-Crown-4 (12CN4) in aqueous solution and its experimental interaction with nano $CuSO_4$. Int. J. Nano Dimens. **8**, 142–158 (2017)

Abdou, W.M., Barghash, R.F., Bekheit, M.S.: Carbodiimides in the synthesis of enamino- and α-aminophosphonates as peptidomimetics of analgesic/antiinflammatory and anticancer agents. J. Arch. Pharm. Chem. Life Sci. **345**, 884–895 (2012)

Akbas, H., Okumus, A., Kılıc, Z., Hokelek, T., Celik, Z.B.: Phosphorus–nitrogen compounds part 27. Syntheses, structural characterizations, antimicrobial and cytotoxic activities, and DNA interactions of new phosphazenes bearing secondary amino and pendant (4-fluorobenzyl)spiro groups. Eur. J. Med. Chem. **70**, 294–307 (2013)

Ali, T.E., Hassan, M.M.: Reaction of 2-cyano-3-(4-oxo-4H-chromen-3-yl)prop- 2-enamide with some phosphorus reagents: synthesis of some novel diethyl phosphonates, 1,2,3- diazaphosphinanes, 1,2,3-thiazaphosphinine and 1,2-azaphospholes bearing a chromone ring. Res. Chem. Intermed. **44**, 173–189 (2018)

Ali, M.A.E.A.A., Kamel, M.S., Abdel Halim, S.H., Shokr, E.K., Abdel-Ghany, H., Hamad, H.: Facile synthesis and photodetection characteristics of new pyrrolo[2,3-b] pyrrole-based metal-free organic dyes containing phenols as the potential candidates towards energy conversion. Mater. Chem. Phys. **293**, 126972–126989 (2023)

Avci, D.: Second and third-order nonlinear optical properties and molecular parameters of azo chromophores: Semiempirical analysis. Spectrochim Acta A **82**, 37–43 (2011)

Avci, D., Başoğlu, A., Atalay, Y.: Ab initio HF and DFT calculations on an organic non-linear optical material. Struct. Chem. **21**, 213–219 (2010)

Dake, S., Raut, A., Kharat, D.S., Mhaske, K.R., Deshmukh, R.S., Pawar, S.M.: Ionic liquid promoted synthesis, antibacterial and in vitro antiproliferative activity of novel α-aminophosphonate derivatives. Bioorg. Med. Chem. Lett. **21**, 2527–2532 (2011)

GaussView, Version 5, Dennington, R., Keith, T., Millam, J. Semichem Inc., Shawnee Mission K.S (2009)

Gnanasambandan, T., Gunasekaran, S., Seshadri, S.: Experimental and theoretical study of p-nitroacetanilide spectrochim. Acta A Mol. Biomol. Spectrosc. **117**, 557–567 (2014)

Göker, H., Boykin, D.W., Yıldız, S.: Synthesis and potent antimicrobial activity of some novel 2-phenyl or methyl-4H-1-benzopyran-4-ones carrying amidinobenzimidazoles. Bioorg. Med. Chem. **13**, 1707–1714 (2005)

Hassanin, N.M., Ali, T.E., El-Shaaer, H.M., Hassan, M.M.: Reaction of 2-imino-2*H*-chromene-3-carboxamide with phosphorus sulfides: Synthesis of novel 2-sulfido-2,3-dihydro-4*H*-chromeno[2,3-*d*][1,3,2] diaza-phosphinines. Phosphorus Sulfur Silicon Relat. Elem. **193**, 651–655 (2018)

Hemalatha, K.S.K., Rukmani, N., Suriyamurthy, B.M., Nagabhushana, N.: Synthesis, characterization and optical properties of hybrid PVA–ZnO nanocomposite: a composition dependent study. Mater. Res. Bull. **51**, 438–446 (2014)

Huang, W., Ding, Y., Miao, Y., Liu, M.Z., Li, Y., Yang, G.F.: Synthesis and antitumor activity of novel dithiocarbamate substituted chromones. Eur. J. Med. Chem. **44**, 3687–3696 (2009)

Larget, R., Lockhart, B., Renard, P., Largeron, M.: A convenient extension of the Wessely–Moser rearrangement for the synthesis of substituted alkylaminoflavones as neuroprotective agents in vitro. Bioorg. Med. Chem. Lett. **10**, 835–838 (2000)

Lee, S.K., Chae, S.M., Yi, K.Y., Kim, N.J., Oh, C.H.: 4-[(N-Imidazol-2-ylmethyl)anilino]pyranopyridine analogs as novel anti-angiogenic agents. Bull. Korean Chem. Soc. **26**, 619–628 (2005)

Long, N., Cai, X., Song, J., Yang, B.A., Chen, S., Bhadury, Z., Lu, P.S., Jin, D.Y., Xue, L.H.W.: Synthesis and antiviral activities of cyanoacrylate derivatives containing an α-aminophosphonate moiety. J. Agric. Food Chem. **56**, 5242–5246 (2008)

Mazzei, M., Sottofattori, E., Dondero, R., Ibrahim, M., Melloni, E., Michetti, M.: N, N-Dialkylaminosubstituted chromones and isoxazoles as potential anti-inflammatory agents. Il Farmaco **54**(7), 452–460 (1999)

Natorajan, S., Shanmugam, G., Martin, S.A.: Growth and characterization of a new semi organic NLO material: L-tyrosine hydrochloride. Cryst. Res. Technal. **43**, 561–564 (2008)

Nohara, A., Ishiguro, T., Ukawa, K., Sugihara, H., Maki, H., Sanno, Y.: Studies on antianaphylactic agents 7. synthesis of antiallergic 5-Oxo-5H-[1]benzopyrano[2,3-b]pyridines. J. Med. Chem. **28**, 559–568 (1985)

Pietta, P.J.: Flavonoids as antioxidants. J. Nat. Prod. **63**, 1035–1042 (2000)

Reed, A.R., Weinstock, R.B., Weinhold, F.: Natural population analysis. J. Chem. Phys. **83**, 735–746 (1985)

Sajan, D.Y., Erdogdu, R., Reshmy, O., Dereli, K., Thomas, K., Hubert, I.: DFT-based molecular modeling, NBO analysis and vibrational spectroscopic study of 3-(bromoacetyl)coumarin. Spectrochim. Acta Part A **82**, 118–125 (2011a)

Sajan, D., Joseph, L., Vijayan, N., Karabacak, M.: Natural bond orbital analysis, electronic structure, nonlinear properties and vibrational spectral analysis of L-histidinium bromide monohydrate: a density functional theory. Spectrochim. Acta A **81**, 85–98 (2011b)

Stadler, S., Feiner, F., Briuchle, C., Brandl, S., Gompper, R.: Determination of the first hyperpolarizability of four octupolar molecules and their dipolar subunits via hyper-Rayleigh scattering in solution. Chem. Phys. Lett. **245**, 292–296 (1995)

Szafran M., Komasa A., Bartoszak-Adamska E.: Crystal and Molecular Structure of 4-Carboxypiperidinium Chloride (4-piperidine-carboxylic acid hydrochloride), J. Mol. Struct. **827**, 101–107 (2007)

Ukawa, K., Ishiguro, T., Kurik, H., Nohara, A.: Synthesis of the metabolites and degradation products of 2-Amino-7-isopropyl-5-oxo-5H-[1] benzopyrano [2, 3-b] pyridine-3-carboxylic acid (Amoxanox). Chem. Pharm. Bull. **33**, 4432–4437 (1985)

Ungwitayatorn, J., Samee, W., Pimthon, J.: 3D-QSAR studies on chromone derivatives as HIV-1 protease inhibitors. J. Mol. Struct. **689**, 99–106 (2004)

Wang, Q., Zhu, M., Zhu, R., Lu, L., Yuan, C., Xing, S., Fu, X., Mei, Y., Hang, Q.: Exploration of α-aminophosphonate N-derivatives as novel, potent and selective inhibitors of protein tyrosine phosphatases. Eur. J. Med. Chem. **49**, 354–364 (2012)

Yanai, T., Tew, D., Handy, N.: A new hybrid exchange–correlation functional using the Coulomb-attenuating method (CAM-B3LYP). Chem. Phys. Lett. **393**, 51–57 (2004)